Springer

KSME

Journal of Mechanical Science and Technology 31 (1) (2017) 63~73
www.springerlink.com/content/1738-494x(Print)/1976-3824(Online)
DOI 10.1007/s12206-016-1208-0

On the dynamics of tapered vibro-impacting cantilever with tip mass†

P. S. Gandhi* and Vishal Vyas

Suman Mashruwala Advanced Microengineering Laboratory, Department of Mechanical Engineering, Indian Institute of Technology - Bombay, Mumai, 400076, India

(Manuscript Received March 7, 2016; Revised July 28, 2016; Accepted August 6, 2016)

Abstract

This paper explores nonlinear dynamic behavior of vibro-impacting tapered cantilever with tip mass with regard to frequency response analysis. A typical frequency response curve of vibro-impacting beams displays well-known resonance frequency shift along with a hysteric jump and drop phenomena. We did a comprehensive parametric analysis capturing the effects of taper, tip-mass, stop location, and gap on the non-smooth frequency response. Analysis is presented in a non-dimensional form useful for other similar cases. Simulation results are further validated with corresponding experimental results for a few cases. Illustrative comparison of simulation results for varying parameters brings out several interesting aspects of variation in the nonlinear behavior.

Keywords: Beam; Frequency response; Jump and drop phenomena; Tapered cantilever; Vibro-impact

1. Introduction

Vibro-impact phenomena play an important role in the dynamic behavior of structural components having motion constraints. Impacting situations occur in a variety of systems because of intermittent contact between mated parts as a consequence of clearances and manufacturing tolerances. Some of the examples of such practical situations include the interaction between bridges and their foundation, impact between gear teeth due to backlash, contact between steam generator tubes and their respective supports during flow induced vibration, reed type valve in refrigeration compressor [1, 2]. The analysis of a vibrating beam with motion constraints provides a good insight into the rich dynamic behavior of these systems. The vibro-impact phenomenon gives rise to complex dynamic behavior and leads to modeling and analysis related challenges. Hence, the vibro-impacting beam has been investigated by numerous researchers by experimental and analytical approaches.

Vibro-impacting uniform beams have been studied extensively to analyze the qualitative behavior of vibro-impacting systems. Moon and Shaw [3] analyzed the chaotic response of vibro-impacting beam for harmonic excitation force. Shaw and Holmes [4] and Shaw [5] presented sub-harmonic and chaotic motions and bifurcations leading to chaos. Nordmark [6] reported grazing bifurcation in impact oscillators. Many researchers have reported the qualitative changes in the behavior with changing parameters of this so-called monostable system vibro-impacting beam. Apart from these, work has been reported towards modeling approaches of vibro-impacting beams. Two approaches are widely used for modeling of vibro-impacting systems [1]. The first uses the coefficient of restitution model, which assumes instantaneous contact between beam and stop [7-9]. The second approach considers a piecewise linear system in which contact is modeled as a linear spring (or spring damper model) and leads to separate equations for beam in contact and out of contact with the stop [1, 4, 5, 10]. In the early investigations related to modeling [3-5, 8, 9], the vibro-impacting beam was modeled as a single degree of freedom system (single degree of freedom oscillator) to check the qualitative response, and the results were also validated experimentally by Refs. [3, 5]. Wagg and Bishop [7] and Wagg [11] captured the response of uniform vibro-impacting beam without tip mass using multiple modes. These theoretical and experimental analyses were focused on the study of chaotic behavior, bifurcation, super harmonic and subharmonic resonances, period doubling and chaos. Krishna and Padmanabhan [2] studied the impacting uniform cantilever without tip mass under two conditions: Two flexible stops at the free end, and two rigid stops at the free end. They presented jump phenomena and hardening spring type behavior in the frequency response. Gandhi and Badkas [12] reported, for the first time, the frequency responses analysis of the vibro-impacting uniform cantilever with tip mass and varying position of the stop. Abbas et al. [13] reported nonlinear behavior and frequency shift in hollow beams filled with metal swarf. Chen et al. [14] detected super harmonic and subhar-

*Corresponding author. Tel.: +91 22 25767519, Fax.: +91 22 25726875
E-mail address: gandhi@iitb.ac.in
† Recommended by Associate Editor Eung-Soo Shin
© KSME & Springer 2017

monic resonances and jump phenomena in the frequency response of the gear system with rectangular mesh stiffness. Viet et al. [15] used frequency response analysis to check the performance of semi-active tuned mass dampers. Numbers of important cases associated with dynamics of vibro-impacting beams are reported in the Refs. [16-21].

Many other researchers have contributed in the study of vibro-impacting systems. However, some areas are still untouched. The previous literature is primarily focused on uniform cantilever beams. However, many vibro-impacting components have varying cross section and can be modeled and investigated as a tapered beam (for example, turbine and compressor blade, reed valve). To the best of our knowledge, the dynamics of a vibro-impacting tapered cantilever has not been explored so far. It is evident that the trends of qualitative behavior of vibro-impacting uniform and tapered beam remain more or less the same, but the quantitative changes due to the taper affect the resonance regimes and oscillation amplitude. We focus on analytical and experimental characterization of the nonlinear frequency response of vibro-impacting tapered cantilever with tip mass and further on its non-dimensional parametric analysis. The analysis is useful in understanding the effects of variable cross sections on the vibro-impact response of the systems. Furthermore, the resonance regimes and oscillation amplitude are the critical parameters in designing the cantilever beam type vibration energy harvesters which have been investigated recently [20]. The analysis provides a base for the future research on exploiting wider bandwidth with high amplitude by changing the geometry of vibro-impacting beam for efficient absorption of ambient vibration.

Theoretical analysis based on assumed modes method and spring damper model for impact stop is employed. According to assumed mode method, the displacement of vibrating beam is expressed as,

$$y(s,t)=\sum_{i=1}^{\infty}\varphi_i(s)q_i(t), \tag{1}$$

where $\varphi_i(s)$ are admissible functions of the spatial variable s (we use $\varphi_i(s)$ as the mode shapes of a tapered beam with tip mass) and $q_i(t)$ are time dependent generalized coordinates. Natural frequencies and mode shapes of tapered beam with varying width and constant thickness cannot be determined analytically. Hence a numerical approach using differential transform applied previously [22-24] is employed for the purpose. Equations of dynamics, obtained using force balance, and simplified using Eq. (1) and orthogonality of mode shapes, are used for simulation and parametric analysis. The results are validated against simulated and experimental results of vibro-impacting uniform cantilever presented in Gandhi and Badkas [12]. Comprehensive simulation results are presented in non-dimensional form towards parametric analysis leading to complete characterization.

This paper is organized as follows: Sec. 2 describes dynamic modeling of vibro-impacting tapered beam with tip mass. The differential transform method used for obtaining natural frequencies and mode shapes is presented. Experimental and simulation details are presented in Sec. 3. Results obtained from the present investigation are discussed in Sec. 4. Finally, Sec. 5 concludes the research work.

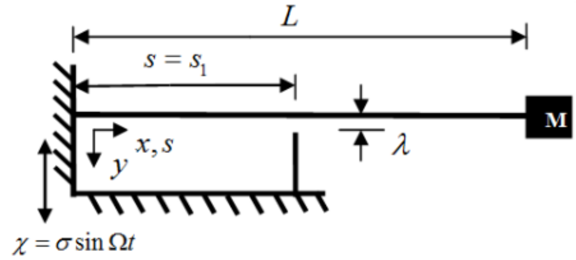

Fig. 1. Schematic of vibro-impact beam.

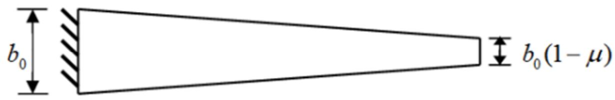

Fig. 2. Top view of beam without end mass.

2. Modeling

Figs. 1 and 2 show schematic diagrams of a linearly tapered vibro-impacting cantilever beam having tip mass. The beam is mounted horizontally and harmonic displacement excitation is given at its fixed end. The stop is placed at one side to restrict the motion of the vibrating beam. The position of the stop can be changed by moving the stop along x direction, and the gap between beam and stop can be adjusted by moving the stop along y direction.

Modeling involves three stages. Subsec. 2.1 presents the governing equation of vibro-impacting non-uniform cantilever beam with tip mass and excited at the fixed end. Modal analysis is carried out in Subsec. 2.2 by using differential transform method to obtain mode shapes to be used in assumed modes method. The last subsection finally uses mode shapes in assumed modes method to obtain uncoupled equations of generalized coordinates.

2.1 Governing equations and solution approach

The cantilever is considered to have the following properties: Linear elastic material having modulus of elasticity E, area moment of inertia *I(x),* cross section area *A(x)* and density ρ . The linear taper variation in width is characterized by taper parameter $\mu(\mu\in[0,1])$. The width $b(x)$ of the beam is expressed in terms of taper parameter μ as,

$$b(x)=b_0u(x)=b_0(1-\mu\frac{x}{L}), \tag{2}$$

where function $u(x)$ represents the variation of width along the length of the beam. If $s=x/l, s\in[0,1]$ is defined as dimensionless length of the beam, then $u(s)=1-\mu s$ represents dimensionless width function. The equation governing the transverse vibration of Euler Bernoulli beam under the effect of distributed viscous damping C and external excitation force $f(x,t)$ is

$$\frac{\partial^2}{\partial x^2}\left[EI(x)\frac{\partial^2 y(x,t)}{\partial x^2}\right]+C\frac{\partial y(x,t)}{\partial t}+\rho A(x)\frac{\partial^2 y(x,t)}{\partial t^2} = f(x,t). \tag{3}$$

In the above equation, $y(x,t)$ denotes the transverse displacement of vibrating beam and $f(x,t)$ is external excitation. For linearly varying width, area moment of inertia $I(x)$ and the area $A(x)$ in terms of dimensionless length s are,

$$\begin{aligned} I(s) &= b_0(1-\mu s) = I_0 u(s), \\ A(s) &= A_0(1-\mu s) = A_0 u(s), \end{aligned} \tag{4}$$

where I_0 and A_0 are the moment of inertia and area, respectively, at the big end of the tapered beam. Considering base excitation, Eq. (3) in non-dimensional coordinates can be written as

$$\begin{aligned} &\frac{\partial^2}{\partial s^2}\left[\frac{EI(s)}{L^4}\frac{\partial^2 y(s,t)}{\partial s^2}\right]+C\frac{\partial y(s,t)}{\partial t} \\ &+\rho A(s)\frac{\partial^2 y(s,t)}{\partial t^2} \\ &= \rho A(s)\frac{\partial^2 \chi}{\partial t^2}, \end{aligned} \tag{5}$$

where the base excitation $\chi=\sigma\sin(\Omega t)$ .When base excitation is given to the beam with the stop placed at a certain position along its length, the dynamics of the beam can be developed considering the following cases:

Case 1. Beam is not in contact with the stop ($y(s_1)<\lambda$).

Case 2. Beam is in contact with the stop ($y(s_1)\ge\lambda$).

When the beam is in contact with the stop (case 2), the impact force comes in action and the governing equation becomes,

$$\begin{aligned} &\frac{\partial^2}{\partial s^2}\left[\frac{EI(s)}{L^4}\frac{\partial^2 y(s,t)}{\partial s^2}\right]+C\frac{\partial y(s,t)}{\partial t} \\ &+\rho A(s)\frac{\partial^2 y(s,t)}{\partial t^2} \\ &= \rho A(s)\frac{\partial^2 \chi}{\partial t^2}+F_{imp}. \end{aligned} \tag{6}$$

Impact stop is modeled by considering it to be a ground spring damper system as shown in Fig. 3. Hence, the external force due to impact can be expressed as,

$$F_{imp} = (K_S(\lambda - y(s_1,t)) - C_S\frac{\partial y(s_1,t)}{\partial t})\delta(s-s_1), \tag{7}$$

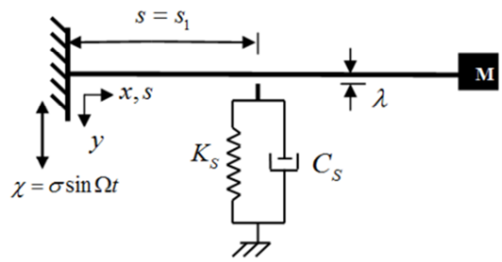

Fig. 3. Schematic of impact stop modeling.

where δ is Dirac delta function and s_1 is the location of stop from the fixed end of the beam. When the beam is not in contact with stop (case 1), Eq. (5) is used, and when the beam is in contact with stop (case 2), Eq. (6) is used to predict the response of the vibrating beam. As mentioned, the assumed mode method is used for simplifying infinite dimensional system Eqs. (5) and (6) to finite dimensions. Eq. (1), considering finite number N of modes, can be written as

$$y(s,t)=\sum_{i=1}^{N}\varphi_i(s)q_i(t), \tag{8}$$

where N is the number of modes assumed. We consider admissible functions $\varphi_i(s)$ as natural mode shapes of a tapered beam. Mode shapes are determined by a numerical method using differential transforms presented in the following section.

2.2 Natural frequencies and mode shapes by differential transform

Considering the homogeneous part of governing Eq. (5) and neglecting damping and applying separation of variable,

$$y(s,t)=\varphi(s)Q(t), \tag{9}$$

where $\varphi(s)$ is mode shape function and $Q(t)$ is temporal coordinate of transverse displacement y, we can get two separate equations for spatial and temporal variable. By putting this value of y in Eq. (5) and neglecting damping and external excitation, we get two equations,

$$\frac{d^2Q(t)}{dt^2}+\omega^2 Q(t)=0, \tag{10}$$

$$\frac{d^2}{ds^2}\left[\frac{EI(s)}{L^4}\frac{d^2\varphi(s)}{ds^2}\right]-\rho A(s)\omega^2\varphi(s)=0. \tag{11}$$

By putting the values of *A(s)* and *I(s)* from Eq. (4), Eq. (11) can be expressed as,

$$\frac{d^2}{ds^2}\left[u(s)\frac{d^2\varphi(s)}{ds^2}\right]-\beta^4 u(s)\varphi(s)=0, \tag{12}$$

where β is dimensionless natural frequency and is defined as,

$$\beta^4 = \frac{\rho A_0 L^4}{EI_0}\omega^2. \tag{13}$$

Eq. (12) can be expanded as,

$$u(s)\frac{d^4\varphi}{ds^4} + 2\frac{du}{ds}\frac{d^3\varphi}{ds^3} + \frac{d^2\varphi}{ds^2}\frac{d^2u}{ds^2} - \beta^4 u(s)\varphi(s) = 0. \tag{14}$$

The boundary conditions for a tapered cantilever with tip mass are,

$$\begin{aligned} & y(0,t) = 0, \\ & \frac{\partial y(0,t)}{\partial s} = 0, \\ & \frac{\partial^2 y(1,t)}{\partial s^2} = 0, \\ & \frac{1}{L^3}\frac{\partial}{\partial s}\left[EI(1)\frac{\partial^2 y(1,t)}{\partial s^2}\right] = M\frac{\partial^2 y(1,t)}{\partial t^2}. \end{aligned} \tag{15}$$

Applying separation of variables, the boundary conditions are converted in form of φ are,

$$\begin{aligned} & \varphi(0) = 0, \frac{d\varphi(0)}{ds} = 0, \\ & \frac{d^2\varphi(1)}{ds^2} = 0, \frac{d^3\varphi(1)}{ds^3} = \frac{-M_r}{(1-\mu)}\beta^4\varphi(1), \end{aligned} \tag{16}$$

where M_r is mass ratio defined as

$$M_r = \frac{M}{\rho A_0 L}. \tag{17}$$

Solving Eq. (14) for boundary conditions Eq. (16) gives the values of nondimensional natural frequencies and mode shapes. Eq. (14) involves variable coefficients and can be solved by numerical methods. The differential transform method is applied here for solution. Differential transform of the function $f(x)$ is defined as [22],

$$F(k) = \frac{1}{k!}\left[\frac{d^k f(x)}{dx^k}\right]_{x=0}. \tag{18}$$

Here, $f(x)$ is the original function and $F(k)$ is the transformed function. Differential inverse transform of $F(k)$ is defined as follows.

$$f(x) = \sum_{k=0}^{\infty} F(k)x^k. \tag{19}$$

By combining Eqs. (18) and (19), we get the following equation.

$$f(x) = \sum_{k=0}^{\infty}\frac{x^k}{k!}\left(\frac{d^k f(x)}{dx^k}\right)_{x=0}. \tag{20}$$

Eq. (20) represents the Maclaurin series of the function $f(x)$. Taking differential transform of Eq. (14) and by using the transformation formula [22, 23], we get the following equation which gives recurrence relation.

$$\begin{aligned} & \sum_{r=0}^{k} U(r)(k-r+1)(k-r+2)(k-r+3) \\ & (k-r+4)\Phi(k-r+4) + 2\sum_{r=0}^{k}(r+1)U(r+1) \\ & (k-r+1)(k-r+2)(k-r+3)\Phi(k-r+3) \\ & +\sum_{r=0}^{k}(r+1)(r+2)U(r+2)(k-r+1) \\ & (k-r+2)\Phi(k-r+2) = \sum_{r=0}^{k}\beta^4 U(r)\Phi(k-r). \end{aligned} \tag{21}$$

$U(k)$ and $\Phi(k)$ are differential transforms of $u(s)$ and $\varphi(s)$, respectively. From transform formulae, the boundary conditions Eq. (16) can be transformed as follows:

$$\Phi(0) = 0, \quad \Phi(1) = 0, \tag{22}$$

$$\sum_{k=0}^{n} k(k-1)\Phi(k) = 0, \tag{23}$$

$$\sum_{k=0}^{n} k(k-1)(k-2)\Phi(k) = -\frac{M_r}{(1-\mu)}\beta^4\sum_{k=0}^{n}\Phi(k), \tag{24}$$

where n is the total number of terms in Maclaurin series. By assuming the symbolic values for $\Phi(2)$ and $\Phi(3)$, we can get other values $\Phi(4)$, $\Phi(5)$,....... $\Phi(n)$ by using recurrence relationship Eq. (21). We assume

$$\Phi(2) = p, \tag{25}$$

$$\Phi(3) = r. \tag{26}$$

Values up to $\Phi(n)$, found by using recurrence relation, are substituted in transformed boundary conditions stated in Eqs. (23) and (24). From two boundary conditions we get two equations in terms of p and r as follows:

$$B_{11}p + B_{12}r = 0, \tag{27}$$

$$B_{21}p + B_{22}r = 0, \tag{28}$$

where B_{11}, B_{12}, B_{21} and B_{22} are polynomials of β corresponding to n terms in Maclaurin series, and for nontrivial solution for p and r we have the following frequency equation in determinant form.

$$\begin{vmatrix} B_{11} & B_{12} \\ B_{21} & B_{22} \end{vmatrix} = 0. \tag{29}$$

By solving Eq. (29), we can get the dimensionless natural frequencies β_i. The accuracy of natural frequencies depends upon the number of terms n used in the series. For lower natural frequencies, convergence occurs even with lower values of n. However, for higher natural frequencies, higher values of n have to be used. The mode shapes are derived by using inverse differential transform. By putting the values of β_i in Eq. (27) or Eq. (28), we can get the ratio $c_i = p/r$. In the differential transform domain, $\Phi^*(k)$ can be obtained by substituting β_i (obtained from Eq. (29)) and $r = p/c_i$ (obtained from Eq. (27) or Eq. (28)) in $\Phi(k)$ (obtained from recurrence relation Eq. (21)). Using these values in inverse differential transform gives $\varphi(s)$ in the dimensionless space coordinate as,

$$\varphi(s) = p\sum_{k=0}^{n} s^k \Phi^*(k). \tag{30}$$

2.3 Dynamics of vibro-impacting beam

After obtaining mode shapes numerically, as mentioned in the previous section, we use Eq. (8) to reduce partial differential equations of motion, to several ordinary differential equations as follows. By putting Eq. (8) in Eq. (5) (No-Impact case) and putting the expression of *I(s)* and *A(s)*,

$$\begin{aligned}&\frac{EI_0}{L^4}\sum_{i=1}^{N}(u(s)\varphi_i(s)'')''q_i(t) + C\sum_{i=1}^{N}\varphi_i(s)\frac{dq_i(t)}{dt}\\&+\rho A_0 u(s)\sum_{i=1}^{N}\varphi_i(s)\frac{d^2q_i(t)}{dt^2}\\&= \rho A_0 u(s)\frac{\partial^2 \chi}{\partial t^2}.\end{aligned} \tag{31}$$

In the above equation, ' represents differentiation with respect to s. By putting the value of $(u(s)\varphi_i(s)'')''$ from the Eq. (12) dividing all the terms by ρA_0 and using the definition of β from Eq. (13), Eq. (31) can be written as,

$$\begin{aligned}&\sum_{i=1}^{N}u(s)\omega_i^2\varphi_i(s)q_i(t) + \frac{2C\omega_i}{2\rho A_0\omega_i}\sum_{i=1}^{N}\varphi_i(s)\frac{dq_i(t)}{dt}\\&+u(s)\sum_{i=1}^{N}\varphi_i(s)\frac{d^2q_i(t)}{dt^2} = u(s)\sigma\Omega^2\sin(\Omega t),\end{aligned} \tag{32}$$

where ω_i is the i^{th} natural frequency corresponding to β_i.

Mode shapes obtained from Eq. (30) are orthogonal to each other. Therefore, if i and j are indices representing the modes and B_i 's are some constants,

$$\begin{aligned}&\int_0^1 u(s)\varphi_i\varphi_j ds = B_i \quad if\ i = j,\\&\int_0^1 u(s)\varphi_i\varphi_j ds \cong 0 \quad if\ i \neq j.\end{aligned} \tag{33}$$

After multiplying Eq. (32) with φ_i and integrating with respect to s in the limit 0 to 1 and using the orthogonality property of mode shapes (Eq. (33)), we get the following independent equations in generalized coordinate q_i for each mode i:

$$\begin{aligned}&\frac{d^2q_i(t)}{dt^2} + \frac{2C\omega_i}{2\rho A_0\omega_i}\frac{dq_i(t)}{dt}\frac{\int_0^1\varphi_i(s)^2 ds}{B_i} + \omega_i^2 q_i(t)\\&= \sigma\omega^2\sin(\Omega t)\frac{\int_0^1 u(s)\varphi_i(s)ds}{B_i}.\end{aligned} \tag{34}$$

We define modal damping factor as,

$$\frac{C}{2\rho A_0\omega_i}\frac{\int_0^1\varphi_i(s)^2 ds}{B_i} = \zeta_i. \tag{35}$$

With this definition, finally, equations of dynamics in terms of generalized coordinates (one for each mode) are given by,

$$\begin{aligned}&\frac{d^2q_i(t)}{dt^2} + 2\omega_i\zeta_i\frac{dq_i(t)}{dt} + \omega_i^2 q_i(t)\\&= \sigma\Omega^2\sin(\Omega t)\frac{\int_0^1 u(s)\varphi_i(s)ds}{B_i}.\end{aligned} \tag{36}$$

Eq. (36) is used when there is no contact with impact stop. By repeating the same procedure on Eq. (6), we can obtain the following equations of dynamics when the cantilever is in contact with the impact stop.

$$\begin{aligned}&\frac{d^2q_i(t)}{dt^2} + 2\omega_i\zeta_i\frac{dq_i(t)}{dt} + \omega_i^2 q_i(t)\\&= \sigma\Omega^2\sin(\Omega t)\frac{\int_0^1 u(s)\varphi_i(s)ds}{B_i}\\&+\frac{1}{\rho A_0 L}\frac{\varphi_i(s_1)}{B_i}(K_S(\lambda - y_1(s_1,t)) - C_S\frac{dy(s_1,t)}{dt})\\&\delta(s - s_1).\end{aligned} \tag{37}$$

Eq. (37) is used during impact.

3. Simulation and experimental details

Using the equations developed in the previous section, dynamics and further parametric analysis is carried out. This section presents important aspects of simulation and experiments. The beam properties (material: Copper beryllium alloy) and nominal dimensions used are listed in Table 1. The values of spring damper parameters *Ks* and *Cs* for impacting stop cannot be taken directly. So the simulations were per-

Table 1. Properties of beam.

Beam properties	Value	Unit
Modulus of elasticity (E)	1.11×10^{11}	N/m^2
Density (ρ)	8200	kg/m^3
Length (L)	150	*mm*
Width at the fixed end (b_0)	16	*mm*
Thickness (h)	0.4	*mm*
Beam damping (ζ)	0.018	
Stop position (s_1)	0.65 (Non-dimensional)	
Stop gap (λ)	1	*mm*
Stop stiffness (K_S)	5500	*N/m*
Stop damping (C_S)	0.00005	*N-s/m*
Excitation amplitude (σ)	0.2	*mm*

formed to decide these values and clarified for better match with experimental results for the case of taper parameter = 0.5 and mass ratio = 0.5 (Fig. 8(c)), and these values were used for simulation for all the other cases. The values used in all the simulations are Ks = 5500 *N/m* and Cs = 0.00005 *Ns/m*. The damping factor ζ_i is found by half power bandwidth method from the experimentally obtained frequency response curve (without stop) for the beam with taper parameters = 0, 0.25, 0.5 and 0.75 and mass ratio = 0.5. The value of average damping factor ζ_i = 0.018 is used in all the simulations. Assuming very small change in the damping with increasing mass ratio, the same damping factor is used for simulations of the beams with mass ratios 1 and 5.

3.1 Simulation details

The equations of dynamics Eqs. (36) and (37) in terms of generalized coordinates are solved using ODE45 solver in MATLAB®. The event detection functionality of the solver is used to locate the event of impact accurately. Convergence analysis is carried out, and first five modes (N = 5 in Eq. (8)) are found to be sufficient to obtain convergence with the desired accuracy. Simulation consisted of slow forward sweep in frequency followed by slow backward sweep with the range around the fundamental frequencies of the beam. At each frequency, the steady state amplitude of the end tip was recorded to finally generate the frequency response.

3.2 Experimental details

Figs. 4 and 5 show a schematic diagram and photograph of the experimental setup, respectively. The beam is clamped horizontally to an aluminum base used as an attachment to a shaker (LDS V406). The impacting stop, screwed in the base, is a M6×0.5 brass fine-threaded screw fitted with steel ball at the tip. Fine threads help in accurately adjusting the stop gap and a locking nut is provided to firmly fix the stop after adjustment. Input signal waveform to the shaker is provided by dSPACE 1104 DAQ system via an amplifier. The excitation

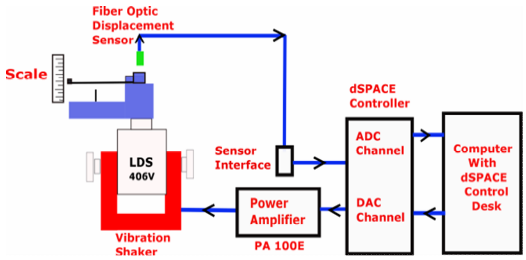

Fig. 4. Line diagram of experimental set-up.

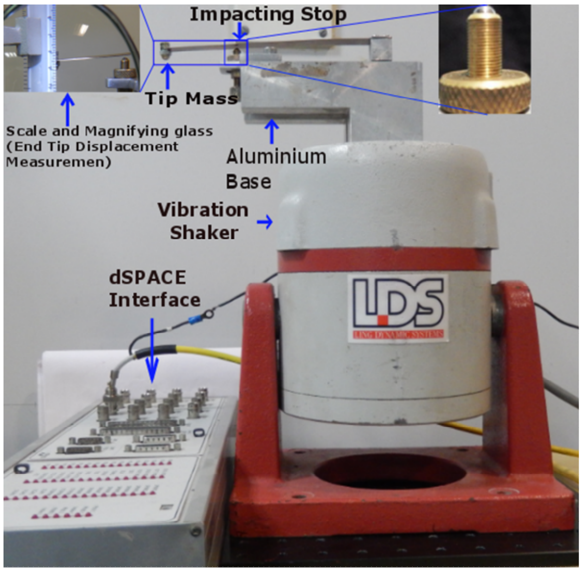

Fig. 5. Experimental set-up.

parameters are adjusted using the dSPACE Controldesk environment. The gain of the amplifier is adjusted to give $\sigma = 0.2\times10^{-3}m$ in all the experiments. A fiber optic displacement sensor (Philtek RC 140) is used to accurately measure small displacement excitation given by the shaker. Large amplitude of the end tip vibration is measured by a scale placed near the end tip as shown in Fig. 4. Although scale gives accuracy of 0.5 *mm* in measurement, error in the measurement is < 2 % because of relatively large tip amplitude. The experiment consists of slow forward sweep followed by slow backward sweep with the range being around the fundamental frequency of the beam. At each frequency, the system is allowed to reach steady state before its response is recorded.

4. Results

4.1 Frequency parameters by DTM

The natural frequencies and mode shapes were obtained by method presented in Sec. 2.2. The natural frequency parameters (β^2) determined by Differential transform method (DTM) were compared with those obtained by Initial value method (IVM) [25] in Table 2. The comparison shows excellent agreement up to two decimal places. The trend of natural frequency parameter shows that when the mass ratio is zero, the natural frequencies increase with increasing taper, but

Table 2. Comparison of natural frequency parameters obtained by Differential transform method (DTM) adopted in this analysis and Initial value method (IVM) [25], where TP = Taper parameter and MR = Mass ratio, i = Mode number.

TP	i	0.3		0.5		0.7	
MR		DTM	IVM	DTM	IVM	DTM	IVM
0	1	3.91	3.91	4.315	4.315	4.931	4.931
	2	22.98	22.98	23.51	23.51	24.68	24.68
	3	62.43	62.43	63.19	63.19	64.52	64.52
1	1	1.533	1.533	1.51	1.511	1.479	1.479
	2	16.43	16.43	16.58	16.58	16.76	16.76
	3	50.99	50.99	51.10	51.10	51.24	51.24
10	1	0.52	0.52	0.505	0.505	0.486	0.486
	2	15.84	15.84	16.10	16.10	16.39	16.39
	3	50.36	50.36	50.61	50.61	50.90	50.90

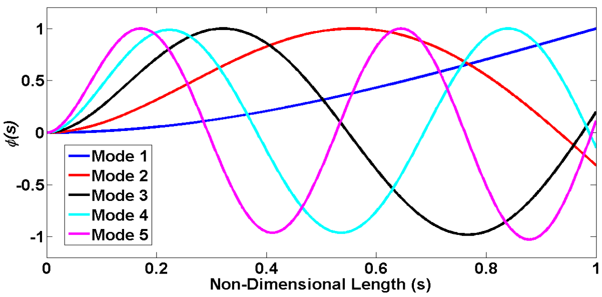

Fig. 6. Mode shapes of tapered cantilever beam with $\mu = 0.25$ and MR = 0.5.

when mass ratio is 1 or 10, the second and third natural frequencies increase with increasing taper, but the first natural frequency decreases with increasing taper. Fig. 6 shows the first five mode shapes obtained by differential transform method for the tapered cantilever with taper parameter $\mu = 0.25$ and mass ratio $MR = 0.5$.

4.2 Validation for a special case

We used the results of the proposed DTM in simulation of trends in nonlinear dynamic behavior and further parametric analysis. Fig. 7 validates simulation results obtained using the proposed DTM method in comparison with previously published [12] simulation results for a special case of uniform cantilever (taper parameter $\mu = 0$).

Mode shapes were obtained analytically in Ref. [12]. The close match between them validates the accuracy of mode shapes obtained by differential transform method in predicting the behavior accurately. Frequency ratio is the ratio of external excitation frequency and resonant frequency of the beam. Amplitude ratio is the ratio of tip amplitude of vibrating beam and base excitation amplitude.

4.3 Parametric analysis

This section presents results of parametric analysis with taper parameters (0, 0.25, 0.5, 0.75) and mass ratios 0.5, 1 and 5.

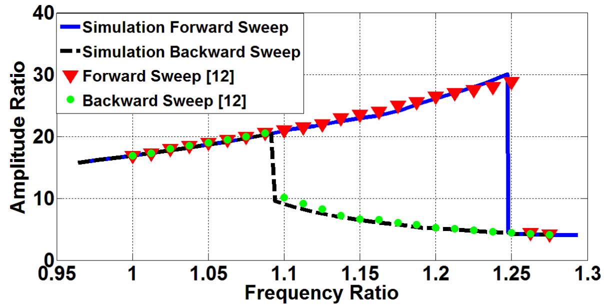

Fig. 7. Comparison of simulation result with the result of Gandhi and Badkas [12] for stop position $s_1 = 0.5$, gap $\lambda = 4$ mm, mass ratio = 1.5 and taper parameter $\mu = 0$. Here frequency ratio $= \Omega / \omega_{n1}$, amplitude ratio $= y_{tip/\sigma}$.

Figs. 8-10 show simulation results for varying taper parameters and mass ratio of 0.5, 1 and 5, respectively. Experimental results are also superimposed for MR = 0.5 for validation purposes. The frequency response curves in all three cases show that for the same mass ratio, as the taper parameter increases, the peak amplitude ratio (highest amplitude ratio in forward sweep curve) and resonance frequency shift increases. The hysteresis region (area between drop and jump line in the frequency response curve) also increases as the taper is increased. The graphs are plotted with the same limits on x and y axes to visually capture the trend. Experimental results for MR = 0.5 match very well with simulation observations. Thus, the taper on cantilever enhances the nonlinear effect of jump and hysteresis phenomena.

Moreover, for the same taper parameter, as the mass ratio is increased, the peak amplitude ratio decreases, but the resonance frequency shift increases. Increased mass would prevent higher amplitudes of vibration, and hence we see the decrease in the peak amplitude ratio. The trend observed above can be explained by the physics of the system. The intensity of impact plays an important role in the evolution of dynamics. This intensity is expressed in terms of impact force exerted by the stop during impact. The last term of right hand side in Eq. (37) represents the impact force I_f expressed as

$$I_f = \frac{1}{\rho A_0 L} \frac{\varphi_i(s_1)}{B_i} (K_S(\lambda - y_1(s_1,t)) - C_S \frac{dy(s_1,t)}{dt}) \delta(s - s_1). \tag{38}$$

When the beam comes in contact with the stop, reaction force I_f is exerted on beam in the opposite direction resulting in change of momentum. In Eq. (38), the term $\varphi_i(s_1)/B_i$ plays a major role in deciding the value of I_f.

As taper parameter increases (for constant mass ratio), $\varphi_i(s_1)/B_i$ increases, which increases the value of the impact force. Increase of impact force further results in higher velocity and displacement of beam, resulting in increase of peak amplitude. The frequency ratio at which a jump is observed remains almost the same in all the cases; thus, increase in peak amplitude happening at higher frequency ratio leads to an increased hysteresis region. With the increase in mass ratio

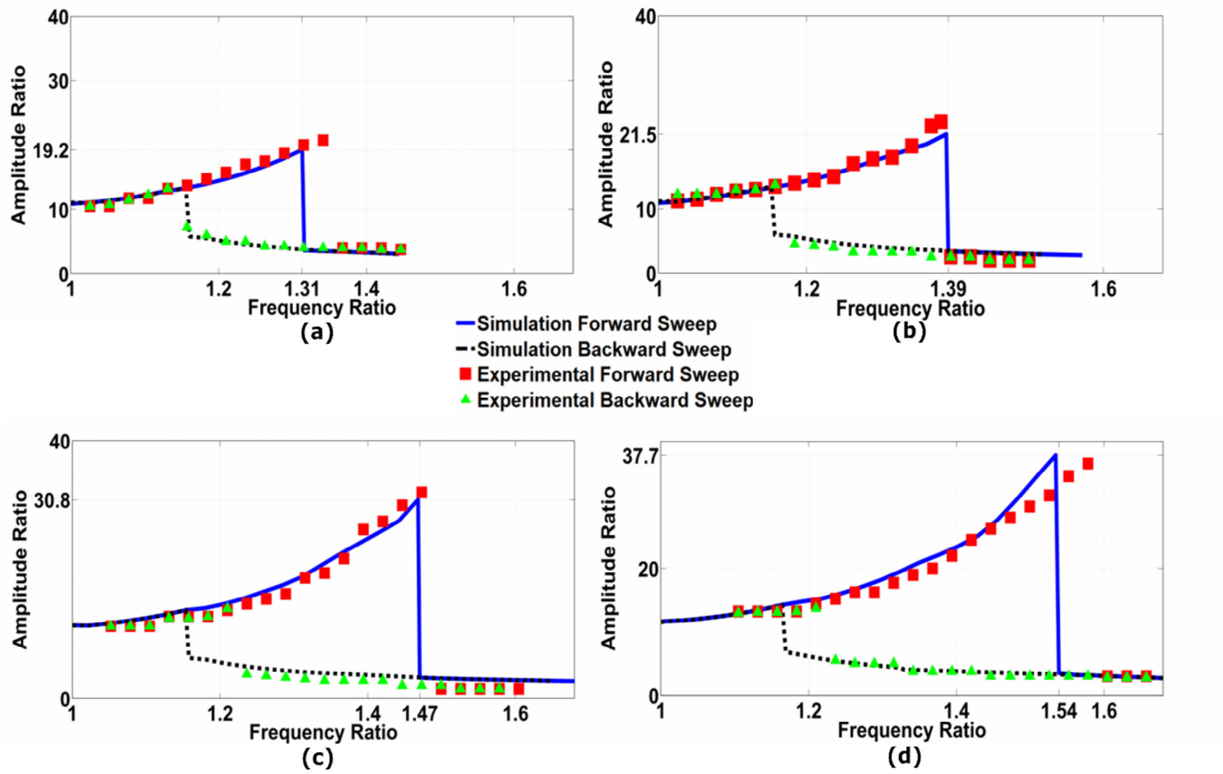

Fig. 8. Simulation and experimental results of frequency response curve for beams with different taper parameters: (a) μ =0; (b) μ =0.25; (c) μ = 0.5; (d) μ =0.75 and mass ratio = 0.5. Here frequency ratio = Ω / ω_{n1} , amplitude ratio = y_{tip} / σ .

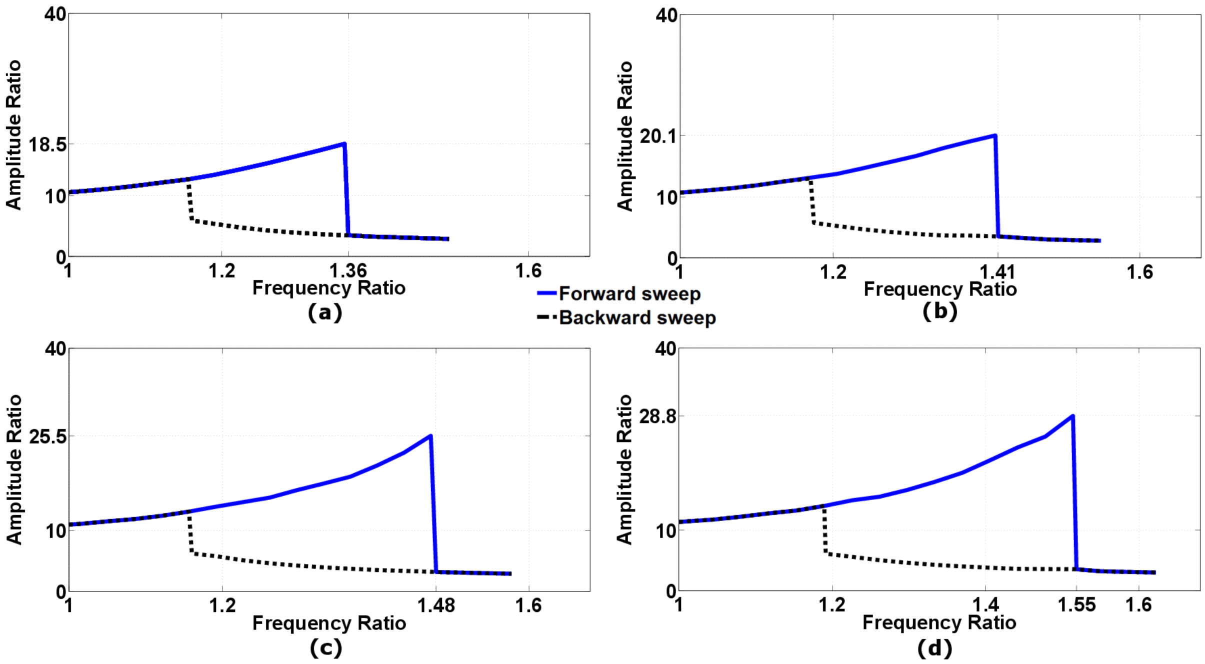

Fig. 9. Simulation results of frequency response curve for beams with different taper parameters: (a) μ = 0; (b) μ = 0.25; (c) μ = 0.5; (d) μ = 0.75 and mass ratio = 1. Here Frequency ratio = Ω / ω_{n1} , amplitude ratio = $y_{tip/\sigma}$.

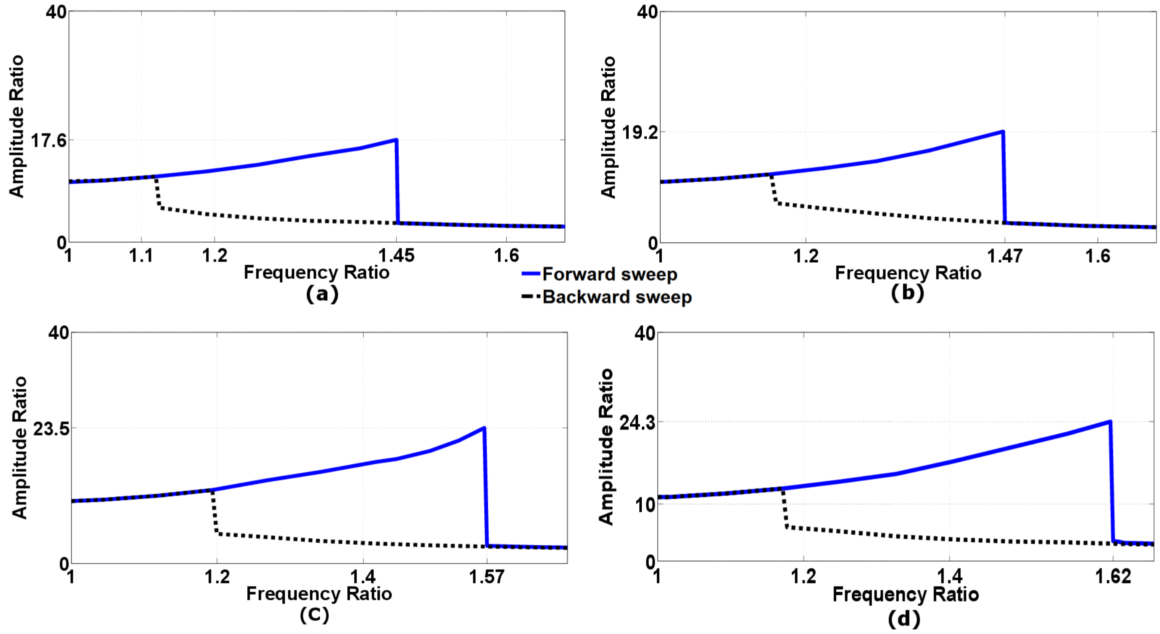

Fig. 10. Simulation results of frequency response curve for beams with different taper parameters: (a) $\mu = 0$; (b) $\mu = 0.25$; (c) $\mu = 0.5$; (d) $\mu = 0.75$ and mass ratio = 5. Here frequency ratio = Ω / ω_{n1} , amplitude ratio = $y_{tip/\sigma}$.

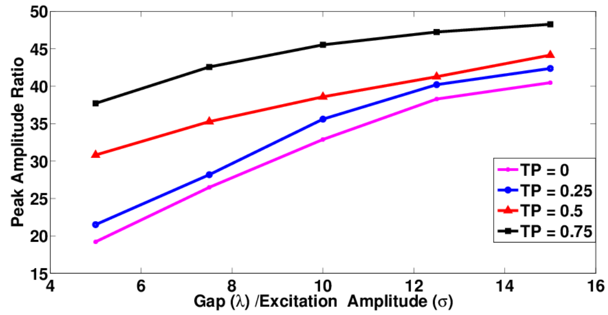

Fig. 11. Change in peak amplitude ratio with respect to gap at various Taper parameters (TP).

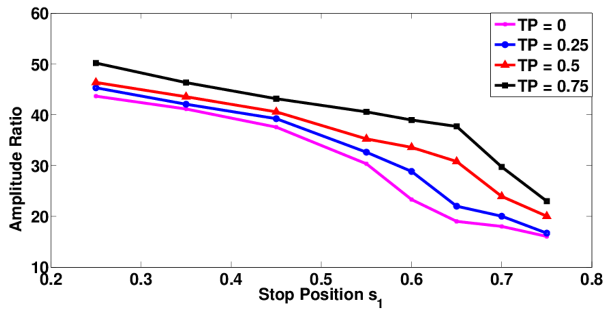

Fig. 12. Change in peak amplitude ratio with respect to stop position s_1 at various Taper parameters (TP).

(for the same taper parameter), the term $\varphi_i(s_1) / B_i$ decreases. Hence, the impact force decreases, which results in less deflection and corresponding lesser amplitude ratio.

Thus, the combination of higher taper parameter with lower mass ratio will give the maximum peak amplitude. Changes in values of K_S and C_S , do not show a significant change in the trend of the results.

Fig. 11 shows the variation in amplitude ratio as the nondimensional gap (λ / σ) increases (stop position is same). The results are shown for the beams with taper parameters 0, 0.25, 0.5 and 0.75 and mass ratio 0.5. As the nondimensional gap increases, the amplitude ratio increases. This behavior can be explained as follows.

With an increase in the gap, the beam can travel more in the downward direction. Hence, the strain energy stored during downward movement increases and the beam gets more kinetic energy during upward movement, thereby increasing the amplitude ratio.

Fig. 12 shows the effect of stop position on the peak amplitude ratio for beams with varying taper parameter and nominal mass ratio 0.5. For the same gap, as the stop moves towards the free end, the peak amplitude ratio decreases. The reason for this behavior is the restricted movement of the vibrating beam in the downward direction as the stop moves towards the free end.

To understand the effect of stop location, consider the vibro-impacting beam MN as shown in Fig. 13 with two different stop locations.

Case 1. Stop location close to fixed end at S_g .

Case 2. Stop location close to free end at S_h .

$O''N''$ *and* $O'N'$ represent the deflected beam segments after the stop location for cases 1 and 2, respectively.

The deflection of the impacting beam for both the cases depends upon the length of $O'N'$ and $O''N''$ and the curva-

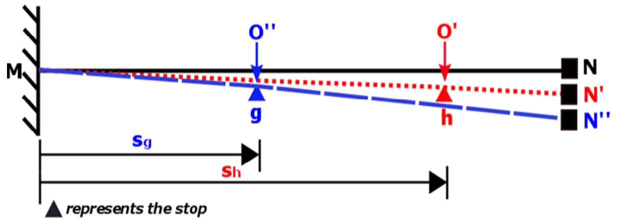

Fig. 13. Effect of stop location on vibro-impacting beam.

ture of segments $O'N'$ and $O''N''$ after impact. However, in the present analysis, the Euler-Bernoulli beam is considered and the deflection is very small compared to the length of the beam. Therefore, the change in curvature of deflected beam segments $O'N'$ and $O''N''$ is negligible. Hence, the length of the beam segments after stop location ($O'N'$ and $O''N''$) is the governing factor which affects the deflection of vibro-impacting beam. Since $O''N''$ is longer than $O'N'$, the deflection of the beam in the positive y direction (Fig. 1) is more in case 1 than in case 2, which is shown in the Fig. 13. Hence, as the stop moves towards the free end the deflection of the tip of vibro-impacting beam decreases.

5. Conclusion

Detailed theoretical and experimental analysis has been carried out to understand the dynamic behavior of the "vibro-impacting tapered beam having tip mass". The analysis is focused on the general trends of frequency response with varying parameters, which provides insight into dynamic characteristics of such systems. The dynamic response of the system is modeled using the assumed mode method and the stop is modeled as a spring damper system. The differential transform method is used to solve for the natural frequencies, and mode shapes of the tapered beam with tip mass and the results are validated with the available literature. Results are presented with non-dimensional parameters to capture the essence of the behavior. The frequency response of the beams with different taper parameters and mass ratios is obtained by simulation and validated with experiments. It has been observed that the peak amplitude ratio at the resonance frequency, resonance frequency shift, and the hysteresis region (area between the jump and drop line in the frequency response curve) increase with increasing taper parameter and decreasing mass ratio.

Further, increasing gap between the beam and stop decreases the intensity of impact and results in decreased resonance frequency shift but increased peak amplitude ratio. Moreover, as the stop location moves away from the fixed end by keeping the gap the same, the peak amplitude ratio decreases and the resonance frequency shift increases. The results would be useful for application areas including vibration energy harvesting and turbo machinery. The analysis method can be extended to vibro-impacting tapered beam with multiple stops and multidimensional cases.

Nomenclature

C : Damping coefficient per unit length ($Ns-m^{-2}$)
M : End mass (kg)
q : Temporal coordinate for transverse displacement m
x,s : Length coordinate (m), dimensionless length coordinate
β : Dimensionless frequency parameter
ζ : Damping Factor
μ : Taper parameter
ρ : Density of beam material ($kg-m^{-3}$)
σ : External excitation (m)
φ : Mode shape function
ω : Natural frequency ($rad-\sec^{-1}$)
Φ : Differential transform of φ
Ω : Frequency of external excitation ($rad-\sec^{-1}$)
A_0 : Area at fixed end of the beam (m^2)
b_0 : Width of beam at fixed end (m)
I_0 : Area moment of inertia at the fixed end of the beam (m^4)
s_1 : Dimensionless distance of point of impact from the fixed end
y_{tip} : Displacement at the tip of the beam (m)
$A(s)$: Variable cross section area of the beam (m^2)
$I(s)$: Variable area moment of inertia of the beam (m^4)

References

[1] K. J. Fegelman and K. Grosh, Dynamics of a flexible beam contacting a linear spring at low frequency excitation: Experiment and analysis, *J. of Vibration and Acoustics,* 124 (2002) 237-249.
[2] I. R. P. Krishna and C. Padmanabhan, Experimental and numerical investigations of impacting cantilever beams part 1: first mode response, *Nonlinear Dynamics,* 67 (2012) 1985-2000.
[3] F. C. Moon and S. W. Shaw, Chaotic vibrations of a beam with non-linear boundary conditions, *Int. J. of Non-Linear Mechanics,* 18 (6) (1983) 465-477.
[4] S. W. Shaw and P. J. Holmes, A periodically forced piecewise linear oscillator, *J. of Sound and Vibration,* 90 (1) (1983) 129-155.
[5] S. W. Shaw, Forced vibrations of a beam with one-sided amplitude constraint: Theory and experiment, *J. of Sound and Vibration,* 99 (2) (1985) 199-212.
[6] A. B. Nordmark, Non-periodic motion caused by grazing incidence in an impact oscillator, *J. of Sound and Vibration,* 145 (2) (1991) 279-297.
[7] D. Wagg and S. Bishop, Application of non-smooth modeling techniques to the dynamics of a flexible impacting beam, *J. of Sound and Vibration,* 256 (5) (2002) 803-820.
[8] S. R. Bishop, M. G. Thompson and S. Foale, Prediction of period-1 impacts in a driven beam, *Proceedings of Royal Society: Mathematical, Physical and Engineering Sciences,* 452 (1954) (1996) 2579-2592.

[9] D. Wagg, G. Karapodinis and S. R. Bishop, An experimental study of the impulse response of a vibro-impacting cantilever beam, *J. of Sound and Vibration,* 228 (2) (1999) 243-264.

[10] A. Fathi and N. Popplewell, Improved approximations for a beam impacting a stop, *J. of Sound and Vibration,* 170 (3) (1994) 365-375.

[11] D. J. Wagg, A note on co-efficient of restitution models including the effects of impact induced vibration, *J. of Sound and Vibration,* 300 (2007) 1071-1078.

[12] P. Gandhi and A. Badkas, On the nonlinear dynamics of a vibro-impacting cantilever with end mass, *ASME 2012 International Mechanical Engineering Congress and Exposition,* American Society of Mechanical Engineers (2012) 253-261.

[13] H. Abbas, H. Hai, J. Rongong and Y. Xing, Damping performance of metal swarfs in a horizontal hollow structure, *J. of Mechanical Science and Technology*, 28 (1) (2014) 9-13.

[14] S. Chen, J. Tang and Z. Hu, Comparisons of gear dynamic responses with rectangular mesh stiffness and its approximate form, *J. of Mechanical Science and Technology*, 29 (9) (2015) 3563-3569.

[15] L. D. Viet, N. B.Nghi, N. N. Hieu, D. T. Hung, N. N. Linh and L. X. Hung, On a combination of ground-hook controllers for semi-active tuned mass dampers, *J. of Mechanical Science and Technology*, 28 (6) (2014) 2059-2064.

[16] S. Wang, Y. Wang, Z. Huang and T. X. Yu, Dynamic behavior of elastic bars and beams impinging on ideal springs, *J. of Applied Mechanics,* 83 (3) (2016) 031002.

[17] X. Long, J. Liu and G. Meng, Nonlinear dynamics of two harmonically excited elastic structures with impact interaction, *J. of Sound and Vibration,* 333 (5) (2014) 1430-1441.

[18] I. R. P. Krishna and C. Padmanabhan, Experimental and numerical investigation of impacting cantilever beams: Second mode response, *International J. of Mechanical Sciences,* 92 (2015) 187-193.

[19] M. Elmegard, B. Krauskopf, K. M. Osinga, J. Starke and J. J. Thomsen, Bifurcation analysis of a smoothed model of a forced impacting beam and comparison with an experiment, *Nonlinear Dynamics,* 77 (3) (2014) 951-966.

[20] K. Vijayan, M. I. Friswell, H. H. Khodaparast and S. Adhikari, Non-linear energy harvesting from coupled impacting beams, *International J. of Mechanical Sciences,* 96 (2015) 101-109.

[21] J. Y. Yoon and B. Kim, Analysis of vibro-impacts in a torsional system under both wide open throttle and coast conditions with focus on the multi-staged clutch damper, *J. of Mechanical Science and Technology*, 29 (12) (2015) 5167-5181.

[22] S. H. Ho and C. K. Chen, Analysis of general elastically end restrained nonuniform beams using differential transform, *Applied Mathematical Modeling,* 22 (1998) 1219-234.

[23] A. Mirzabeigy, Semi-analytical approach for free vibration analysis of variable cross-section beams resting on elastic foundation and under axial force, *International J. of Engineering,* 26 (3) (2014) 385-394.

[24] M. Malik and H. H. Dang, Vibration analysis of continuous systems by differential transformation, *Applied Mathematics and Computation,* 96 (1998) 17-26.

[25] C. Y. Wang, Vibration of a tapered cantilever of constant thickness and linearly tapered width, *Arch. Appl. Mech.,* 83 (2013) 171-176.

P. S. Gandhi received his Ph.D. from Rice University, Houston, TX. He is currently a Professor at Indian Institute of Technology-Bombay, Mumbai, India. His research interests are in nonlinear dynamics and control, MEMS fabrication, robotics and mechatronics.

Vishal Vyas is a Ph.D. student in the Mechanical Engineering Department, Indian Institute of Technology-Bombay, Mumbai, India. His research interests are in nonlinear vibrations of continuous systems and vibration energy harvesting.